Journal of Materials Chemistry A

Accepted Manuscript

ROYAL SOCIETY OF CHEMISTRY

www.rsc.org/materialsA

Aligned polyaniline nanowires grown on internal surface of macroporous carbon for supercapacitors

Jianpeng Li, Yaqi Ren, Zhonghua Ren, Shuguang Wang, Yejun Qiu*, and Jie Yu*

Shenzhen Engineering Lab for Supercapacitor Materials, Shenzhen Key Laboratory for Advanced Materials, Department of Material Science and Engineering, Shenzhen Graduate School, Harbin Institute of Technology, University Town, Shenzhen 518055, China.
*Corresponding author. E-mail: yejunqiu@hitsz.edu.cn, jyu@hitsz.edu.cn
Keywords: macroporous carbon, polyaniline nanowires, internal surface, supercapacitor, specific capacitance

Abstract

High utilization efficiency of electrode materials is of great importance for achieving excellent electrochemical performance of supercapacitors. In this paper, we report growth of aligned polyaniline (PANI) nanowires on internal surface of macroporous carbon (MC) derived from luffa sponge fibers for increasing their utilization efficiency. The pores in the MC are densely packed, straight, and parallel with the diameter at micrometer scale, which provide easy paths for reaction solution to penetrate and thus enable growth of the PANI nanowires on the internal wall surface. Due to full exposure towards electrolyte the PANI nanowires exhibit high utilization efficiency, leading to high specific capacitance up to 1500 F g^{-1} (1 A g^{-1}). As the macropores allow easy penetration of the electrolyte the PANI nanowires show high rate capability with the capacitance retention up to 70% with increasing the current density from 1 to 10 A g^{-1}. Symmetric supercapacitors assembled using the MC/PANI materials possess high energy density (19 Wh kg^{-1} at 0.5 kW kg^{-1}) and long cycle life (83% retention after 7000 cycles). Considering the abundance and green production of the luffa sponge the MC/PANI composites are promising for industrial application of supercapacitors.

1. Introduction

Supercapacitors (SCs) are gaining rapidly increasing attention for their high promise as next generation energy storage devices.[1-2] However, the SCs suffer from low energy density comparing with Li-ion batteries, which in turn hinders their industrial application.[3] The performance of SCs inclusive of energy density mainly depends on the type and structure of electrode materials. Among the different electrode materials polyaniline (PANI) has received considerable interest due to the relatively high conductivity[4] and largest theoretical pseudocapacitance.[5] PANI belongs to the typical pseudocapacitive materials, which stores energy by Faradaic reaction involving multiple redox states.[6] However the pseudocapacitive reactions occur only on surface layers contacting electrolyte with the inner part inactive as dead volume. Therefore, increasing the active sites exposed towards the electrolytes is of great importance for increasing the utilization efficiency and thus the specific capacitance of PANI. A great number works have been devoted to increasing the utilization efficiency and specific capacitance of PANI by making it into nanomaterials with small size and good dispersion. For example, high specific capacitances up to 1739 F g^{-1} was obtained when dispersing PANI on graphene.[7] The highest specific capacitance so far reported (3407 F g^{-1}) was obtained by growing the aligned PANI nanorods on ITO substrates.[8] However, this value was obtained at relatively low mass loading of 0.1076 μg cm^{-2}, which is far from the requirement of practical application.[8] At present, PANI are generally grown on various carbon nano-supports such as graphene/CNFs,[9] CNTs/CNFs,[10] mesoporous carbon,[11] graphene,[12] carbon nanotubes (CNTs),[13] and carbon nanofibers (CNFs) [14,15] for improving the dispersion and electrical conductivity. Another typical strategy to increase the utilization efficiency is to grow aligned PANI nanowires on various conducting substrates.[8,16-21] By these designs the contacting area of PANI with the electrolytes are effectively increased, resulting in the increase of the utilization efficiency. Furthermore, the gap formed between the PANI nano-units provides easy paths for the electrolytes to penetrate deep into the electrodes, further enhancing the utilization efficiency.[17] However, it is noted that for the previous reports the PANI nanomaterials were generally grown or supported on the outer surface of the supports. In this case, the active materials may contact or aggregate with each other or with the conductive and bond additives during application, which will decrease the exposed sites and thus the utilization efficiency of PANI. Therefore, we here propose to grow the PANI nanomaterials on the internal surface of macroporous carbon (MC) for further increasing the utilization efficiency and obtaining high specific capacitance.

Recently, we prepared the MC from luffa sponge fibers.[22,23] Inherited from the natural structure of the luffa sponge fibers, the MC possesses densely packed , straight, parallel, and completely through channels with diameters ranging from several to over ten micrometers and thickness less than 2 μm. It is expected that the large pore size and fluent pore structure allows free access of the reaction solution, enabling full coverage growth of the PANI nanomaterials on the internal surface of the MC. In this work, we prepared aligned PANI nanowires on internal surface of the MC derived from the luffa sponge fibers for SC application. The PANI nanowires were obtained

by *in situ* polymerization of aniline monomers. Because of easy access of the reaction solution the PANI nanowire arrays were successfully grown on the internal pore walls of the MC. Because of the full exposure towards the electrolyte solution the PANI nanowires grown on the internal surface of the MC (MC/PANI) have high utilization efficiency, resulting in high specific capacitance. The PANI nanowires exhibit high specific capacitances up to 1500 F g^{-1} (based on the mass of the PANI nanowires in the composite) and high capacitance retention of 72% when increasing the current density from 1 to 10 A g^{-1}. The symmetric SCs assembled using the MC/PANI composites possess a high energy density of 19 Wh kg^{-1} at 0.5 kW kg^{-1} (based on the total mass of the MC/PANI composite) and high cycling stability with the capacitance retention at 83% after 7000 cycles. Considering the abundance of the luffa sponge the present MC/PNAI materials are highly promising for SC application.

2. Experimental section

2.1 Materials

Ammonium peroxydisulfate (APS), perchloric acid ($HClO_4$), and aniline monomer were purchased from Aladdin Chemistry Co. Ltd (Shanghai, China). The luffa sponge fibers were supplied by South China Plant Home (Guangzhou). All the chemicals were used as received without further purification or modification.

2.2 Preparation of MC

A certain amount of luffa sponge fibers was heated at 800 ºC in NH_3 atmosphere for 2 h at a heating rate of 5 ºC min^{-1}. Subsequently, the above obtained carbon products were mixed with KOH at a mass ratio of 1:2, and then heated at 750 ºC for 1.5 h in N_2 atmosphere to generate porous surface, obtaining the MC. Finally, the MC samples were washed with 1M HCl solution and distilled water to remove the residue impurities.

2.3 Preparation of MC/PANI

30 mg of the MC was dispersed in 50 mL of 1 M $HClO_4$ cold aqueous solution by ultrasonic stirring, and then a certain amount of the aniline monomer (0.036, 0.109, 0.146, 0.219, 0.365, and 0.730 mL) was added into the above suspension with ultrasonic stirring for 3 h to ensure complete dispersion of the aniline on the MC. Subsequently, 30 mL of 1 M $HClO_4$ cold aqueous solution mixed with 0.1369 g APS was rapidly added into the above suspension under ultrasonic stirring. After reacting for 9 h, the MC/PANI particles were collected from the solution by filtering and then washed with deionized water for several times. Finally, the above obtained MC/PANI particles were dried at 60 ºC for 12 h. The molar ratio of aniline to APS was kept at 2:1 for all the experiments. The concentrations of the aniline monomer in the reaction solutions are 5, 15, 20, 30, 50, and 100 mM, corresponding to the adding amount of 0.036, 0.109, 0.146, 0.219, 0.365, and 0.730 mL, respectively. According to the aniline concentration applied in the reaction solution the obtained samples were denoted as MC/PANIX, where X represents the initial concentrations of the aniline monomer. For comparison, pure PANI nanowires were also synthesized in the absence

of MC via similar procedures.

2.4 Characterization

The morphology of the samples was observed with a field-emission scanning electron microscope (FESEM, Hitachi S-4700). X-ray diffraction (XRD) measurements were conducted on a Rigaku D/max 2500PC diffractometer with nickel-filtered Cu Kα radiation of λ=0.154 nm. Fourier transform infrared (FTIR) spectra were recorded on a Thermo NIR-Antaris II FTIR spectrometer in the range of 4000−450 cm^{-1}. Raman spectra were recorded using a micro-Raman spectroscope with the excitation wavelength of 532 nm (Renishaw RM-1000). X-ray photoelectron spectroscopy (XPS) analyses were performed using an ESCALAB 250 system (VG Scientific Co., Ltd., UK). Nitrogen sorption isotherms were measured at 77 K with a Micromeritics Tristar 3000 analyzer (USA). Before measurements, the samples were degassed in vacuum at 200 ºC for 6 h. The specific surface area was calculated by the Brunauer–Emmett–Teller (BET) method.

2.5 Electrochemical measurement

The electrochemical properties of the samples were measured on a three-electrode system in 1 M H_2SO_4 solution, where a platinum wire (CHI115), an Ag/AgCl (sat.) (CHI111) electrode, and the MC/PANI samples were used as the counter, reference, and working electrode, respectively. For preparing the working electrodes, 8 mg of the MC/PANI powders and 1 mg of carbon black were mixed in 1 mL ethanol to form a slurry. Then an appropriate amount of the slurry was spread onto the surface of a glassy carbon electrode and dried in air. Afterwards, a drop of nafion solution (5 wt.%) was dripped onto the dried slurry for fixation, obtaining the working electrodes.

The SCs were assembled by using the MC/PANI15, aluminum foils, glass fiber papers (NKK separator, Nippon Kodoshi Corporation), and 1 M H_2SO_4 aqueous solution as the electrode materials, current collectors, separators, and electrolyte, respectively. For preparing the electrodes, 9 mg of the MC/PANI15 powders, 0.83 mg of polytetrafluoroethylene (dispersed in water at 60 wt %) as binder, and 0.5 mg carbon black as conductive additive were blended together in ethanol homogeneously to form a slurry. Then an appropriate amount of the slurry was pressed onto the aluminum foils followed by drying at 80 °C in vacuum for 12 h, obtaining the electrodes. Before assembling the SCs the glass fiber paper separators were soaked in 1 M H_2SO_4 solution for 1 h, which were then sandwiched between two of the above prepared electrodes. In the next step, the above sandwich structure was put into the coin battery shells with the edge sealed using polyvinylidene fluoride insulating gel.

Cyclic voltammogram (CV) curves, galvanostatic charge/discharge (CD) curves, and electrochemical impedance spectra (EIS) were measured on a CHI 760D electrochemical work station (Shanghai CH Instruments Co., China). The EIS spectra were measured in the frequency range of 0.01–100 kHz with an AC perturbation of 5 mV. The operation stability was measured by a battery measuring system (CT2001A, Wuhan Land Electronics Co. Ltd.).

The specific capacitance, energy density, and power density of the active materials

or SCs were calculated by the following equations, respectively:

$$C_{MCPA} = \frac{I \times \Delta t}{m \times \Delta V} \quad (1)$$

$$C_{PA} = (C_{MCPA} - C_{MC} * C\%) / PA\% \quad (2)$$

$$E = \frac{1}{2} \times C_{MCPA} \times (\Delta V)^2 \quad (3)$$

$$P = \frac{E}{\Delta t} \quad (4)$$

In the above equations the meanings of the used symbols are explained as follows. C_{MCPA} (F g^{-1}) is the specific capacitance of the MC/PANI composites. I (A), ΔV (V), and Δt (s) are the current, potential window, and time of discharge, respectively. m (g) is the mass of the MC/PANI composites. C_{MC} (F g^{-1}) is the specific capacitance of the MC before growing the PANI. C_{PA} (F g^{-1}) is the specific capacitance of the PANI in the MC/PANI composites. *C%* and *PA%* are the weight percentages of the MC and PANI in the composites, respectively, which were calculated from the weight difference between the original MC and the MC/PANI composites. E (Wh kg^{-1}) is the energy density (converting to Wh kg^{-1} after divided by 3.6) and P (W kg^{-1}) is the power density.

3. Results and discussion

The MC was prepared from the luffa sponge fibers by carbonization in NH_3 and activation in N_2 successively. Even after sever heat treatment the fiber morphology and macroporous structure of the luffa sponge precursor were well preserved (Fig. S1).[22,23] The macropores are densely packed, straight, parallel, and completely through with diameters at micrometer scale (Fig. S1). Fig. 1 shows the SEM images of the MC/PANI prepared at the aniline concentrations of 15 and 20 mM. It is observed that after the growth reaction the original pore structure of the MC did not change (Fig. 1a). The PANI was successfully grown on both the outer surface and the internal wall surface of the MC (Fig. 1b). From the image taken from a freshly fractured cross section it is clearly observed that the PANI was successfully grown on the internal wall surface of the macropores (Fig. 1c), demonstrating the full coverage growth of the PANI on the internal surface of the MC. When observing at higher magnification (Fig. 1d) it is seen that the PANI coatings are composed of aligned nanowires perpendicular to the wall surface with the length in 130-200 nm (Fig. 1e). In our experiments, it is found that the growth and morphology of the PANI nanowires are dependent on the concentration of aniline solution (Fig. S2). At the aniline concentration of 5 mM shorter and scattered PANI nanowires are produced. At the aniline concentrations of 15 and 20 mM the diameters of the nanowires are 15-25 nm and 26-35 nm (Fig. 1d and f and Fig. S2), respectively. The MC/PANI composites were also prepared at the aniline concentrations of 30, 50, and 100 mM (Fig. S2). It is observed that at the aniline concentration of 30 mM some randomly oriented nanowires appear on the aligned nanowires. However, with increasing the aniline

concentration to 50 and 100 mM only randomly oriented nanowires are observed on the surface with sequentially increased diameter. It is also observed that the aligned nanowires became denser with increasing the aniline concentration and even form continuous film at the aniline concentration of 30 mM (Fig. S2), which is disadvantageous to the charge storage due to loss of the electrolyte transfer path. In addition, we found that the pure PANI prepared without MC is randomly oriented nanowires with diameter of 35-70 nm and length of 0.5-2 μm (Fig. S3). These results indicate that at lower aniline concentrations (5, 15, and 20 mM) only heterogeneous nucleation occurs, resulting in the growth of the PANI nanowires only on the MC. At higher aniline concentrations (30, 50, and 100 mM) homogeneous nucleation occurs simultaneously,[16] where the obtained products are the mixture of the MC/PANI and the disordered nanowires polymerized in liquid phase. In order to ensure the PANI nanowires to grow only on the MC and avoid appearance of the liquid-phase grown disordered nanowires we prepared the MC/PANI composites at the aniline concentrations of 15 and 20 mM in this work.

FTIR spectroscopy was used to get information on the chemical bond structure of the samples. As can be seen in Fig. 2a, the spectrum of the MC (spectrum I) shows peaks at 3432, 1639, 1387, and 1029 cm^{-1}, corresponding to the H–O–H bending and O–H stretching of the absorbed H_2O molecules, carboxyl O–H stretching, and alkoxy C–O stretching,[21] respectively. Compared with the MC, a group of typical peaks corresponding to PANI appears in the spectra of MC/PANI (spectra III and IV). The peaks at 1577 and 1481 cm^{-1} are C=C stretching vibration of the quinoid rings and benzenoid rings,[24] respectively. The peaks at 1302, 1238, 1118, and 801 cm^{-1} are attributed to the C–N stretching vibration of aromatic amines, C=N stretching in the PANI, and in-plane and out-of-plane bending of C-H in aromatic rings.[11,18,24] The spectra of the MC/PANI15 and MC/PANI20 show about similar peaks to that of the pure PANI (spectrum II).

Raman spectra were measured to further characterize the structure of the samples. As shown in Fig. 2b, the Raman spectrum of the MC displays two prominent peaks at 1333 and 1599 cm^{-1} (spectrum I), which are the so-called D and G peaks characteristic of the carbon structure, respectively. The D peak is assigned to the A_{1g} zone-edge phonon induced by the disorder arising from the finite crystalline size and the G peak arises from the crystalline graphite due to the zone-center E_{2g} mode.[14] After coating PANI a serials of new peaks appear (spectra III and IV), which are similar to that of pure PANI (spectrum II). The peaks at 1162, 1195, and 1242 cm^{-1} are ascribed to C−H bending of the quinoid ring,[10] C-H bending of the benzenoid ring,[25] and C-N stretching mode of the PANI,[26] respectively. The peaks at 1343, 1401, 1484, and 1594 cm^{-1} are attributed to the C-$N^{\cdot+}$ stretching vibration, electronic absorption of free charge carriers,[27] C=N stretching of the quinoid ring, and C–C stretching of the benzenoid ring of PANI,[10,25] respectively. The Raman peaks associated with PANI increase as the concentration of aniline increases, suggesting the corresponding increase of the coated PANI. The PANI dominated Raman spectrum of the MC/PANI20 confirms the full coverage growth of the PANI nanowires on the MC.

Fig. 2c presents the XRD patterns of the different samples. The MC shows two

diffraction peaks at 23.5° and 43.7°, corresponding to the diffraction of (002) and (100) planes of graphitic structure, respectively. The interlayer spacing calculated from the (002) peak is 0.378 nm. After growing the PANI nanowires some new peaks appear. For the MC/PANI20 sample, the new peaks appear at 18.8, 20.4, and 25.0°. The peaks at 18.8 and 25.0° can be ascribed to the periodicity parallel and perpendicular to the polymer chain of PANI,[28] respectively. The peak at 20.4° is due to the layers of polymer chains at alternating distances.[20,28] This pattern is characteristic of the partially crystallized PANI. The diffraction peaks related to PANI decrease with decreasing the aniline concentration, which is obviously caused by the mass decrease of the PANI grown at lower aniline concentration. Interestingly, it is found that the crystallinity of the PANI in the MC/PANI composites is higher than the pure PANI, suggesting that the MC substrates may promote crystallization of PANI.

XPS spectra were measured to further identify the bond structure of the samples. The survey spectra indicate that both MC and MC/PANI samples contain C, O, and N elements (Fig. S4). The N in the MC mainly originates from the carbonization atmosphere NH_3. In addition, a Cl peak was observed in the survey spectrum of the MC/PANI, which indicates that the PANI is Cl doped.[29] The presence of Cl in the MC/PANI is due to the application of $HClO_4$ during polymerization process. The bonding states of C and N were identified by deconvoluting C1s and N1s peaks (Fig. 3). The C1s peak of the MC (Fig. 3a) can be deconvoluted into three Gaussian peaks at 284.4, 284.9, and 286.0 eV, corresponding to the C-C, C-N, and C-O bond,[30] respectively. The C1s peak of the MC/PANI can be deconvoluted into three peaks at 284.7, 285.0, and 286.8 eV, corresponding to the C=C, C–N, and C-O bond in PANI (Fig. 3b),[30] respectively. By deconvoluting the N1s peaks it was found that the N element in the MC is in the forms of pyridinic-N (N-6), pyrrolic-N (N-5), graphitic-N (N-Q), and pyridine-N-oxide (N^+O) with the corresponding peaks at 398.4, 400.1, 401.2, and 403.7 eV (Fig. 3c),[31] respectively, while the N in the MC/PANI is in the forms of imine-like structure (-C=N-), neutral amine-like structure (-NH-), and positively charged structure (-NH^+-) with the corresponding peaks at 398.8 eV, 399.7, and 400.6 eV (Fig. 3d),[25,32] respectively. The N1s peak in the MC/PANI composite is obviously from the coated PANI.

The supercapacitive performance of the MC, PANI, and MC/PANI were first evaluated by CV, EIS, and galvanostatic CD curves in the three electrode system in 1 M H_2SO_4 electrolyte. During the electrochemical measurements the mass loading of the MC/PANI materials is 2.45 mg cm^{-2}. The CV curves of different samples at a scan rate of 5 mV s^{-1} are shown in Fig. 4a. The CV curve of the MC displays a quasi-rectangular shape, indicating that its capacitance mainly originates from the charge accumulation at the electrode/electrolyte interface. The CV curves of the pure PANI, MC/PANI15, and MC/PANI20 exhibit two pairs of redox peaks, which result from the reversible structure conversion of PANI (A1/A2 peaks correspond to the reversible conversion between leucoemeraldine and emeraldine and B1/B2 peaks correspond to that between emeraldine and pernigraniline). The CV current response of the MC/PANI15 increases greatly after growth of PANI on the MC. However, with further increasing the aniline concentration to 20 mM the current response decreases.

This may mainly result from the increased diameter and length of the nanowires, which increases the charge transport resistance and decreases the utilization efficiency of the nanowires. Fig. 4b shows the CV curves of the MC/PANI15 at different scan rates. It is observed that the shape of the CV curves changes not much with increasing the scan rate, indicating the good rate capability of the active materials. The dependence of the CV curves on the scan rate was also tested for the MC, pure PANI nanowires, and MC/PANI20 samples (Fig. S5). It is indicated that the rate capability of the PANI could be greatly improved by growing on the MC due to improvement of the electrical conductivity. The MC/PANI15 shows better rate capability than the MC/PANI20, which results from the decrease of the resistance due to the size decrease of the nanowires at lower aniline concentration.

Fig. 4c shows the EIS spectra of the different samples. For all the spectra a semicircle can be observed in the high frequency region. The high frequency intercept of the semicircle with the real axis represents the equivalent series resistance (R_s) of the system mainly consisting of the bulk resistance of the electrolyte solution and intrinsic resistance of the active materials, in which the former is usually predominant.[33-35] The diameter of the semicircle reflects the magnitude of the interfacial charge transfer resistance (R_{ct}).[17,33] The transition sections between the semicircle and the tail straight line signify the Warburg impedance W_d, which describes the ion diffusion process from solution into the electrode structure.[21,35] The tail straight lines in the lower frequency region are representative of the ion diffusion in the electrode structure, which should be vertical to the real axis for ideal capacitive behavior.[36,37] It is found that the PANI, MC/PANI15, and MC/PANI20 have about similar R_s values at 0.59, 0.46, and 0.62 Ω**,** respectively. This is because the intrinsic resistance of the electrolyte solution is constant. The diameters of the semicircles are 8.19, 1.81, and 4.62 Ω for PANI, MC/PANI15, and MC/PANI20, respectively. Obviously, MC/PANI15 shows the smallest R_s and R_{ct} and highest slope of the tail straight line, indicating fast ion diffusion/transfer process for this sample. It is further revealed that growth on the internal surface of the MC, smaller size, and appropriate separation for the PANI nanowires are preferred for promoting the ion diffusion/transfer process. In order to quantitatively analyze the EIS spectra equivalent circuits were fitted to simulate the experimental data of the different samples (Fig. 4e and S6). The equivalent circuit shown in Fig. 4e is typical of the MC/PANI composites. This equivalent circuit comprises different elements corresponding to different components of the system or charge behaviors, which include the equivalent series resistance (R_s), the pseudocapacitance of the PANI nanowires (CPE1), the charge transfer resistance (R_{ct}), the double-layer capacitance on PANI nanowires (CPE2), the double-layer capacitance from the MC (CPE3), the contact resistance (R_c) between PANI nanowires and MC, and a Warburg diffusion element (W_d).[19,38] The fitting values of the above elements are listed in Table 1. It is found that the fitting values such as R_s, R_{ct}, and CPE1 are well consistent with the experimental data (see below), testifying the high accuracy of the fitting result.

Fig. 4d displays the galvanostatic CD curves of the samples, which all present triangular shape. However, the CD curves of the pure PANI and MC/PANI exhibit

nonlinearity with obvious slope change. This arises from the pseudoreactions of PANI occurring during the charge/discharge processes. The specific capacitances calculated from the discharge curves are 212, 211, 662, and 477 F g^{-1} at the current density of 1 A g^{-1} for the MC, PANI, MC/PANI15, and MC/PANI20, respectively. The specific capacitances of the samples at different current densities are summarized in Table 2, where the specific capacitance of PANI in the MC/PANI composites was calculated by subtracting the contribution of the MC substrates according to the equation (2). It is seen that the PANI nanowires grown on the internal surface of MC possess very high specific capacitance ranging from 1500 to 1082 F g^{-1} at the current densities from 1 to 10 A g^{-1} for the MC/PANI15. It is worth noting that this high specific capacitance was obtained at high mass loading of the active materials. The specific capacitance of 1500 F g^{-1} is higher than the values recently reported such as the electrodeposited PANI on graphene (751.3 F g^{-1} at 1 A g^{-1}),[39] PANI encapsulated in TiO_2 (732 F g^{-1} at 1 A g^{-1}),[19] PANI nanowires on Au plate (950 F g^{-1} at 1 A g^{-1}),[17] PANI on graphene (875 F g^{-1}, 10 mv s^{-1}),[40] and PANI on TiO_2 nanotube arrays (380 F g^{-1} at 0.5 A g^{-1}).[41] It should be pointed out that the present specific capacitances of PANI were considerably underestimated as the contribution of the MC substrates in the MC/PANI composites should be much smaller than the original MC due to the surface coverage by the PANI coatings. In order to explore the origin of the specific capacitance of the MC/PANI composites the specific surface areas of the different samples were measured, which are 1510, 36, 61, and 44 m^2 g^{-1} for the MC, PANI, MC/PANI15, and MC/PANI20 (Fig. S7), respectively. It is indicated that the MC possesses a high specific surface area due to activation, which accounts for its high specific capacitance (212 F g^{-1} at 1 A g^{-1}). After coating with the PANI nanowires the specific surface areas of the MC/PANI15 and MC/PANI20 composites decreased dramatically to be negligible, indicating that the capacitances of the composites are contributed by the pseudoreactions of PANI.

Table 1 Fitting data of the different elements in the equivalent circuit shown in Fig. 4e and S6.

Element	PANI	MC/PANI15	MC/PANI20
R_s (Ω)	0.51	0.48	0.46
R_{ct} (Ω)	7.36	1.55	3.20
CPE1 (F/g)	268.6	1434.0	746.0
CPE2 (F)	2.51×10^{-5}	2.69×10^{-5}	2.69×10^{-5}
CPE3 (F)	—	1.29×10^{-3}	2.22×10^{-4}
R_c (Ω)	—	0.17	1.42
W_d ($S\cdot sec^{0.5}$)	0.11	5.77×10^{-2}	0.21

In addition to high specific capacitance the MC/PANI also possesses excellent rate capability. From Table 2 it is found that the capacitance retention is as high as 70% with increasing the current density from 1 to 10 A g^{-1} for the MC/PANI15, higher than the reported PANI-based materials such as graphene oxide/PANI (40.9%, 0.2-2 A g^{-1}),[16] PANI/expanded graphite nanosheets (50%, 1-8 A g^{-1}),[20] graphene/PANI (61.5%, 1-10 A g^{-1}),[25] and graphene/ZrO_2/PANI (57.3%, 0.3-2 A^{-1}).[21] This indicates that the

charge transfer resistance of PANI can be greatly decreased by growing on the internal surface of the MC besides increasing the utilization efficiency.

It is clearly demonstrated that the PANI nanowires grown on the internal surface of the MC possess excellent electrochemical performance for SC application including high specific capacitance and high rate capability. We speculate that three factors account for the excellent performance of the present PANI nanowires, i.e. growing on the internal surface, large pore size of the MC, and nanowire structure. The growth on the internal surface ensures full exposure of the PANI nanowires to the electrolyte, the large pore size allows easy access of the electrolyte, and the nanowire structure provides short diffusion path of the electrolyte ions. In particular, the factor of growing on the internal surface of the MC plays key roles in improving the electrochemical performance of the active materials. Due to the growth on internal surface the PANI nanowires are able to be fully exposed towards the electrolytes, avoiding the loss of the active surface area caused by stacking or aggregation of the active material, binder, and conductive additive particles. Furthermore, as the PANI nanowires locate on the internal surface of the MC they are not in contact with other particles and thus avoid the damage due to squeezing of adjacent particles during application, leading to high cycling stability.

Table 2 Specific capacitances of the MC, MC/PANI15, MC/PANI20, and PANI in the MC/PANI composites at different current densities. (The mass percentages of PANI in MC/PANI15 and MC/PANI20 composite are 35% and 46%, respectively.)

Sample	Specific capacitance of the MC and composites (F g^{-1})				Specific capacitance of the PANI in composites (F g^{-1})			
	1 A g^{-1}	2 A g^{-1}	5 A g^{-1}	10 A g^{-1}	1 A g^{-1}	2 A g^{-1}	5 A g^{-1}	10 A g^{-1}
MC	212	195	181	169				
MC/PANI15	662	634	570	464	1500	1436	1272	1082
MC/PANI20	478	432	362	309	791	702	562	518

In order to further investigate the application of the MC/PANI composites symmetric SCs were fabricated using the MC/PANI15 sample as it possesses the highest specific capacitance among the different samples. Fig. 5a displays the CV curves of the assembled SC measured at different scan rates, which exhibit a pair of broad redox peaks at around 0.45 V in the positive scan and 0.20 V in the negative scan, indicating the pseudocapacitive characteristics of PANI. Similar to other reports,[42,43] the two couples of redox peaks in the CV curves measured in the two-electrode system are not pronounced compared to those measured in the three-electrode system. It is found that the shape of the CV curves keeps almost unchanged with increasing the scan rate from 5 mV s^{-1} to 100 mV s^{-1}, indicating fast charge transfer process. The galvanostatic CD curves of the SC measured at different current densities are shown in Fig. 5b, which present evident slope changes due to the pseudoreactions. The specific capacitance of the SC calculated based on the total mass of the MC/PANI composites is 138 F g^{-1} at the current density of 1 A g^{-1}. It is found that the specific capacitance remains at 90 F g^{-1} at a high charge/discharge rate of 10 A g^{-1}, retaining 65% of the capacitance at 1 A g^{-1}. The energy density and power

density of the SC were calculated from the discharging curves, as shown in the Ragone plot in Fig. 5c. The energy density can reach 19 Wh kg^{-1} at a power density of 0.5 kW kg^{-1} and remains at 13 Wh kg^{-1} at a high power density of 5 kW kg^{-1}. These values are higher than those for the SCs fabricated using the PANI/carbon composite materials in most reports.[44-46] Cycling stability test indicates that the capacitance retention after 2000 cycles is about 90% and 83% after 7000 cycles at 2 A g^{-1} and the capacitance keeps almost stable after 1000 cycles (Fig. 5d), which is much higher than the capacitance retention of 58.8% of the SC assembled using the pure PANI nanowires (Fig. S8). This improvement results from the uniform supporting of the nanowires on the internal surface of the MC, which ensures the active materials to be fully exposed all through the charge/discharge process. Such cycling performance is comparable to or higher than most of the PANI-related SC devices reported previously such as PANI/CNFs (90%, 5000 cycles),[18] PANI/graphene (91.4%, 5000 cycles, asymmetric SCs),[38] PANI/3D graphene (85.6%, 5000 cycles),[47] PANI/graphene (80%, 800 cycles),[48] PANI/SWCNTs (80%, 1000 cycles),[49] PANI/graphene/CNTs (82%, 1000 cycles, asymmetric SCs),[50] PANI/3D graphene (83%, 5000 cycles),[51] and PANI/graphene (68.7%, 1000 cycles).[52] According to the previous reports,[17,18,21,25,32,39] it is considered that the initial capacitance loss was caused mainly by two factors. Firstly, the PANI swells and shrinks due to doping and de-doping during the charge/discharge processes,[17,21,32,39] resulting in the loss of the active materials by breaking, peeling, and cracking of some fragile parts. Secondly, irreversible reaction may occur initially for some functional groups,[18,21,25] which causes the capacitance loss. We have also calculated the Coulombic efficiency of the charge/discharge process for the SCs for further understanding the cycling performance, as shown in Fig. 5d. It is observed that the Coulombic efficiency is only 72% for the first cycle, which increases gradually to about 90% after 2300 cycles and 100% after 5000 cycles. This changing trend of the Coulombic efficiency is well consistent with that of the specific capacitance. The equivalent series resistance of the SC still keeps at low level after the cycling test (Fig. 5e), suggesting the mechanical stability of the PANI nanowires grown on the internal surface of the MC. By using two SCs in series, different light-emitting diodes (LED) with red, yellow, green, and blue color can be successfully lit after charging at a current density of 2 A g^{-1} (Fig. 5f), indicating the application potential of the MC/PANI materials. As the present process fabricating the SCs is compatible to the industrial manufacturing technique and the luffa sponge fibers is abundant, green, and renewable the MC/PANI composites are of high promise for practical application.

4. Conclusion

In conclusion, aligned PANI nanowires have been grown on the internal surface of the MC prepared from luffa sponge fibers. The MC comprises parallel, densely packed, and completely through pores at micrometer-scale, enabling free access of the reaction solution and hence growth of the PANI nanowires on the internal walls. Likewise, because the large pores allow easy access of the electrolyte the PANI nanowires grown on internal surface of the MC are able to be fully exposed towards

the electrolyte, resulting in high utilization efficiency and high specific capacitance. The symmetric SCs assembled using the MC/PANI materials possess excellent electrochemical performance with high energy density and high cycling stability. The concept for increasing utilization efficiency of active materials by growing on internal surface of the MC is also of significance for other applications such as catalysts and lithium-ion batteries.

Acknowledgements

This work is supported by the National Basic Research Program of China (2012CB933003), National Natural Science Foundation of China (No. 51272057), and Shenzhen Basic Research Program (JCYJ20130329150737027).

Supplementary data

Supplementary data associated with this article can be found in supporting information.

Notes and references

1 P. J. Hall, M. Mirzaeian, S. I. Fletcher, F. B. Sillars, A. J. R. Rennie, G. O. Shitta-Bey, G. Wilson, A. Cruden and R. Carter, *Energy Environ. Sci*., 2014, **3**, 1238-1251.

2 A. S. AricÒ, P. Bruce, B. Scrosati, J. M. Tarascon and W. V. Schalkwijk, *Nat. Mater*., 2005, **4**, 366-377.

3 L. Zhao, Y. J. Qiu, J. Yu, X. Y. Deng, C. L. Dai and X. D. Bai, *Nanoscale*, 2013, **5**, 4902-4909.

4 W. G. Li and M. X. Wan, Porous polyaniline films with high conductivity, *Synthetic Met*., 1998, **92**, 121-126.

5 H. L. Li, J. X. Wang, Q. X. Chu, Z. Wang, F. B. Zhang and S.C. Wang, *J. Power Sources*, 2009, **190**, 578-586.

6 B. E. Conway, V. Birss and J. Wojtowicz, *J. Power Sources*, 1997, 66, 1-14.

7 Y. F. Wang, X.W. Yang, L.Q and D. Li, *Energy. Environ. Sci*., 2013, **6**, 477–481.

8 B. K. Kuila, B. Nandan, M. Böhme, A. Janke and M. Stamm, *Chem. Commun.*, 2009, **14**, 5749–5751.

9 Z. Zhou and X. F. Wu, *J. Power Sources*, 2014, **262**, 44-49.

10 Z. Zhou, X. F. Wu and H Hou, *RSC Adv*., 2014, **4**, 23622-23629.

11 L. X. Li, H. H. Song, Q. C Zhang, J. Y. Yao and X. H. Chen, *J. Power Source*, 2009, **1**, 268-274.

12 K. Zhang, L. L. Zhang, X. S. Zhao and J. S. Wu, *Chem. Mater.*, 2010, **22**, 1392–1401.

13 V. Gupta and N. Miura, *Electrochim. Acta*, 2006, **52**, 1721–1726.

14 Y. J. Qiu, J. Yu, G. Fang, H. Shi, X.S Zhou and X. D. Bai, *J. Phys. Chem. C*, 2009, **113**, 61–68.

15 M. Kotal, A. K. Thakur and A. K. Bhowmick, *ACS Appl. Mater. Interfaces*, 2013, **5**, 8374−8386.

16 J. J. Xu, K. Wang, S. Z. Zu, B. H. Han and Z. X. Wei, *ACS Nano*, 2010, **4**,

5019–5026.
17 K. Wang, J. Y. Huang and Z. X. Wei, *J. Phys. Chem. C*, 2010, **114**, 8062–8067.
18 P. P Yu, Y. Z. Li, X. Y. Yu, X. Zhao, L. H. Wu and Q.H. Zhang, *Langmuir*, 2013, **29**, 12051-12058
19 K. Y. Xie, J. Li, Y. Q. Lai, Z. A. Zhang, Y. X. Liu, G. G. Zhang and H.T. Huang, *Nanoscale*, 2011, **3**, 2202-2207.
20. Y. Z. Li, X. Zhao, P. P. Yu and Q. H. Zhang, *Langmuir*, 2013, **29**, 493−500.
21 S. Giri, D. Ghosh and C. K. Das, *Adv. Funct. Mater*., 2014, **24**, 1312–1324.
22 J. P. Li, Z. H. Ren, Y. Q. Ren, L. Zhao, S. G. Wang and J. Yu, *RSC Adv*., 2014, **4**, 35789 - 35796.
23 J. P. Li, S. G. Wang, Y. Q. Ren, Z. H. Ren, Y. J. Qiu and J. Yu, *Eletrochemic. Acta*, 2014, **149,** 56-64.
24 J. T. Zhang, J. Wang, J. Yang, Y. L. Wang and M. B. Chan-Park, *ACS Sustainable Chem. Eng*., 2014, **2**, 2291-2296.
25 Z. Q. Tong, Y. N. Yang, J. Y. Wang, J. P. Zhao, B. L. Su and Y. Li, *J. Mater. Chem. A*, 2014, **2**, 4642–4651.
26 M. Lapkowski, K. Berrada, S. Quillard, G. Louarn, S. Lefrant and A. Pron, *Macromolecules*, 1995, **28**, 1233-1238.
27 Z. X. Wei, M. X. Wan, T. Lin and L. M. Dai, *Adv. Mater*., 2003, **15**, 136-139.
28 J. P. Pouget, M. E. Jozefowicz, A. J. Epstein, X. Tang and A. G. MacDiarmid, *Macromolecules*, 1991, **24**, 779-789.
29 G. P. Hao, F. Hippauf, M. Oschatz. F. M. Wisser, A. Leifert, W. Nickel, N. Mohamed-Noriega, Z. K. Zheng and S. Kaskel. *ACS Nano*, 2014, **8**, 7138-7146.
30 S. B. Kulkarni, U. M. Patil, I. Shackery, J. S. Sohn, S. Lee, B. Park and S. C. Jun, *J. Mater. Chem. A*, 2014, **2**, 4989-4998.
31 H. B. Wang, T. Maiyalagan and X. Wang, *ACS Catal*., 2012, **2**, 781-794.
32 H. L. Wang, Q. L. Hao, X. J. Yang, L. D. Lu and X. Wang, *Nanoscale*, 2010, **2**, 2164–2170.
33 L. Zhao, J. Yu, W. J. Li, S. G. Wang, C. L. Dai, J. W. Wu, X. D. Bai and C.Y. Zhi, *Nano Energy*, 2014, **4**, 39-48.
34 L. L. Zhang and X. S. Zhao, *Chem. Soc. Rev*., 2009, **38**, 2520–2531.
35 B. G. Choi, J. Hong, W. H. Hong, P. T. Hammond and H. Park, *ACS Nano*, 2011, **5**, 7205–7213.
36 R. B. Rakhi, W. Chen, D. Cha and H. N. Alshareef, *Nano Lett*., 2012, **12**, 2559-2567.
37 W. Chen, R. B. Rakhi, L. B. Hu, X. Xie, Y. Cui and H. N. Alshareef, *Nano Lett*. 2011, **11**, 5165–5172.
38 J. L. Shen, C. Y. Yang, X. W. Li and G. C. Wang, *ACS Appl. Mater. Interfaces*, 2013, **5**, 8467−8476.
39 M. Yu, Y. X. Ma, J. H. Liu and S. M. Li, *Carbon*, 2015, **87**, 98-105.
40 P. Sekar, B. Anothumakkool and S. Kurungot, *ACS Appl. Mater. Interfaces*, 2015, **7**, 7661−7669.
41 S. Xie, M. Y. Gan, L. Ma, Z. T. Li, J. Yan, H. Yin, X. Y. Shen, F. F. Xu, J. Y. Zheng, J. Zhang and J. L. Hu, *Electrochim. Acta*, 2014, **120**, 408-415.

42 M. D. Stoller and R. S. Ruoff, *Energy Environ. Sci*., 2010, **3**, 1294–1301.
43 K. Wang, P. Zhao, X. M. Zhou, H. P. Wu and Z. X. Wei, *J. Mater. Chem*., 2011, **21**, 16373-16378.
44 G. Otrokhov, D. pankratov, G. Shumakovich, M. Khlupova, Y. Zeifman, I. Vasil'eva, O. Morozova and A. Yaropolov, *Electrochim. Acta*, 2013, **123**, 151-157.
45 B. Anothumakkool, A. A. T. Torris, S.N. Bhange, S. M. Unni, M. V. Badiger and S. Kurungot, *ACS. Appl. Mater. Interfaces*, 2013, **5**, 13397-13404.
46 S. B. Sydulu, S. Palaniappan and P. Srinivas, *Electrochim. Acta*, 2013, **95**, 251-259.
47 K. Chi, Z. Y. Zhang, J. Xi, Y. G. Huang, F. Xiao, S. Wang and Y. Q. Liu, *ACS Appl. Mater. Interfaces*, 2014, **6**, 16312−16319.
48 Q. Wu, Y. X. Xu, Z. Y. Yao, A. R. Liu and G. Q Shi, *ACS Nano*, 2010, **4**, 1963–1970 .
49 Z. Q. Niu, P. S. Luan, Q. Shao, H. B. Dong, J. Z. Li, J. Chen, D. Zhao, L. Cai, W. Y. Zhou, X. D. Chen and S. S. Xie, *Energy Environ. Sci*., 2012, **5**, 8726–8733.
50 Q. Cheng , J. Tang, N. Shinya and L. C. Qin, *J. Power Sources*, 2013, **241**, 423-428.
51 P. P Yu, X. Zhao, Z. L. Huang, Y. Z. Li and Q. H. Zhang, *J. Mater. Chem. A*, 2014, **2**, 14413–14420.
52 Z. Y. Gao, F. Wang, J. L. Chang, D. P. Wu, X. R. Wang, X. Wang, F. Xu, S. Y. Gao and K. Jiang, *Electrochim. Acta*, 2014, **133**, 325–334.

Figures and captions

Fig. 1 SEM images of the MC/PANI prepared at the aniline concentrations of 15 mM (a-e) and 20 mM (f): (a) end surface of a MC/PANI fiber at low magnification, (b) end surface of a MC/PANI fiber at high magnification, (c) freshly fractured cross section of a MC/PANI fiber, (d) morphology of the PANI nanowires, (e) cross section showing the height of the nanowires, (f) morphology of the PANI nanowires.

Fig. 2 FTIR spectra (a), Raman spectra (b), and XRD patterns (c) of different samples: (I) MC, (II) pure PANI, (III) MC/PANI15, (IV) MC/PANI20.

Fig. 3 (a) C1s peak of MC, (b) C1s peak of MC/PANI, (c) N1s peak of MC, (d) N1s peak of MC/PANI.

Fig. 4 Electrochemical charcterization of different samples: (a) CV curves of different samples at a scan rate of 5 mV s^{-1}, (b) CV curves of MC/PANI15 at different scan rates, (c) EIS spectra of different samples (The inset shows the enlarged spectra in high frequency region), (d) Galvanostatic CD curves of different samples at a current density of 1 A g^{-1}. (e) Equivalent circuit for simulating the EIS spectra of the MC/PANI sample. (I-MC, II-pure PANI, III-MC/PANI15, IV-MC/PANI20).

Fig. 5 (a) CV curves of the SC at different scan rates, (b) galvanostatic CD curves of the SC at different current densities, (c) Ragone plots of the symmetric SC device, (d) cycling performance and the corresponding Coulombic efficiency of the SC at a charge/discharge current density of 2 A g^{-1}, (e) Nyquist plots of the SC before and after cycling test, (f) photographs of the LEDs driven by the SCs.

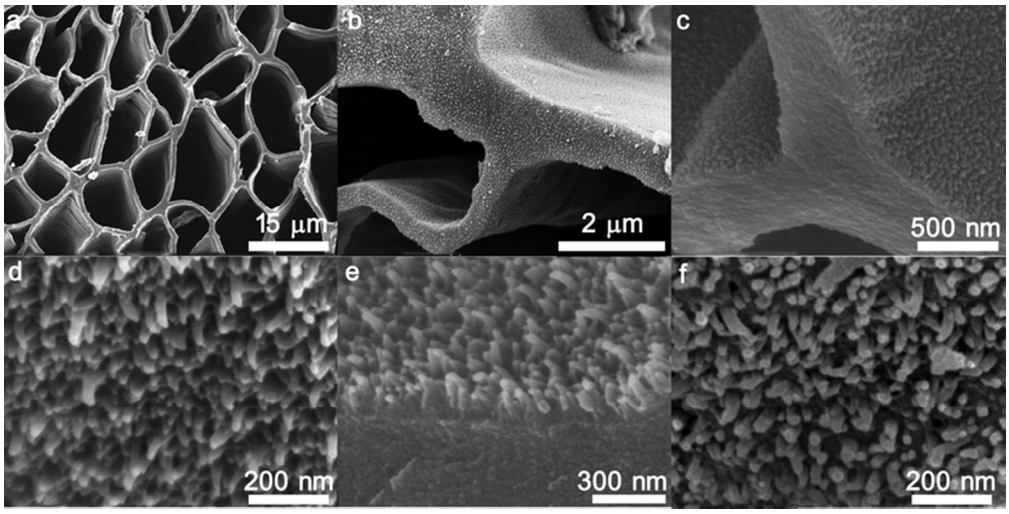

Fig. 1 SEM images of the MC/PANI prepared at the aniline concentrations of 15 mM (a-e) and 20 mM (f): (a) end surface of a MC/PANI fiber at low magnification, (b) end surface of a MC/PANI fiber at high magnification, (c) freshly fractured cross section of a MC/PANI fiber, (d) morphology of the PANI nanowires, (e) cross section showing the height of the nanowires, (f) morphology of the PANI nanowires.
70x35mm (300 x 300 DPI)

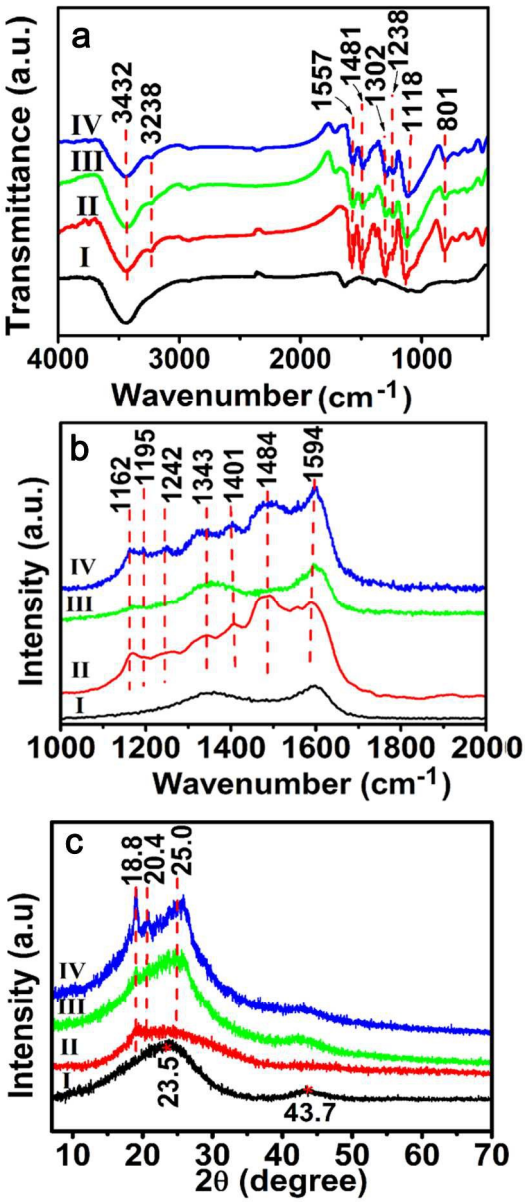

Fig. 2 FTIR spectra (a), Raman spectra (b), and XRD patterns (c) of different samples: (I) MC, (II) pure PANI, (III) MC/PANI15, (IV) MC/PANI20.
180x405mm (300 x 300 DPI)

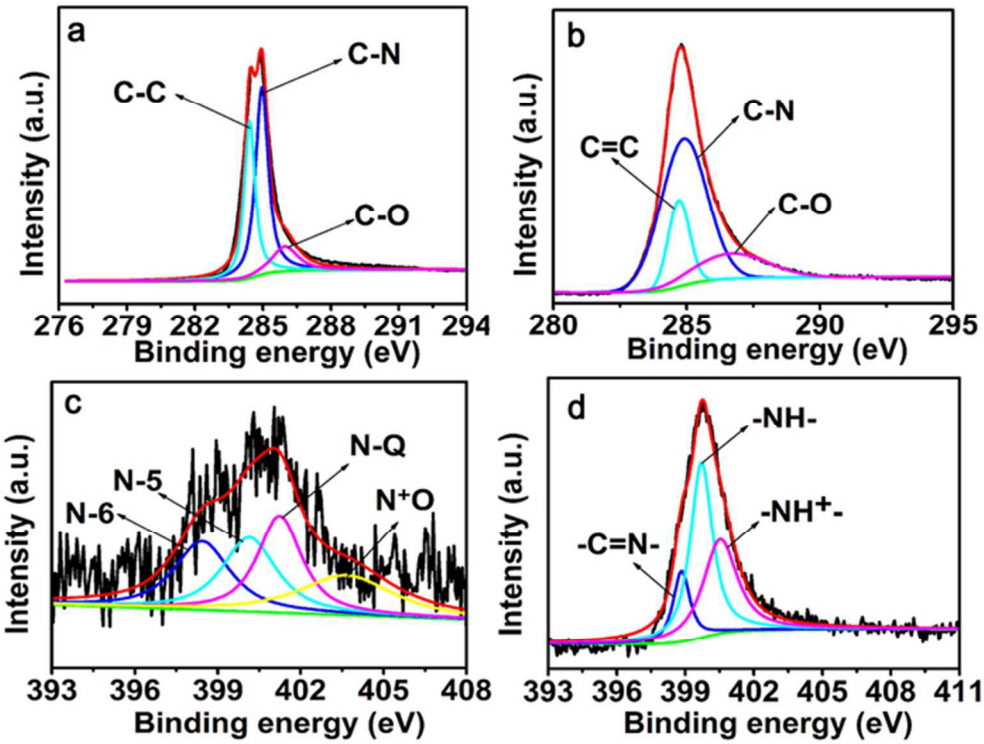

Fig. 3 (a) C1s peak of MC, (b) C1s peak of MC/PANI, (c) N1s peak of MC, (d) N1s peak of MC/PANI.
59x44mm (300 x 300 DPI)

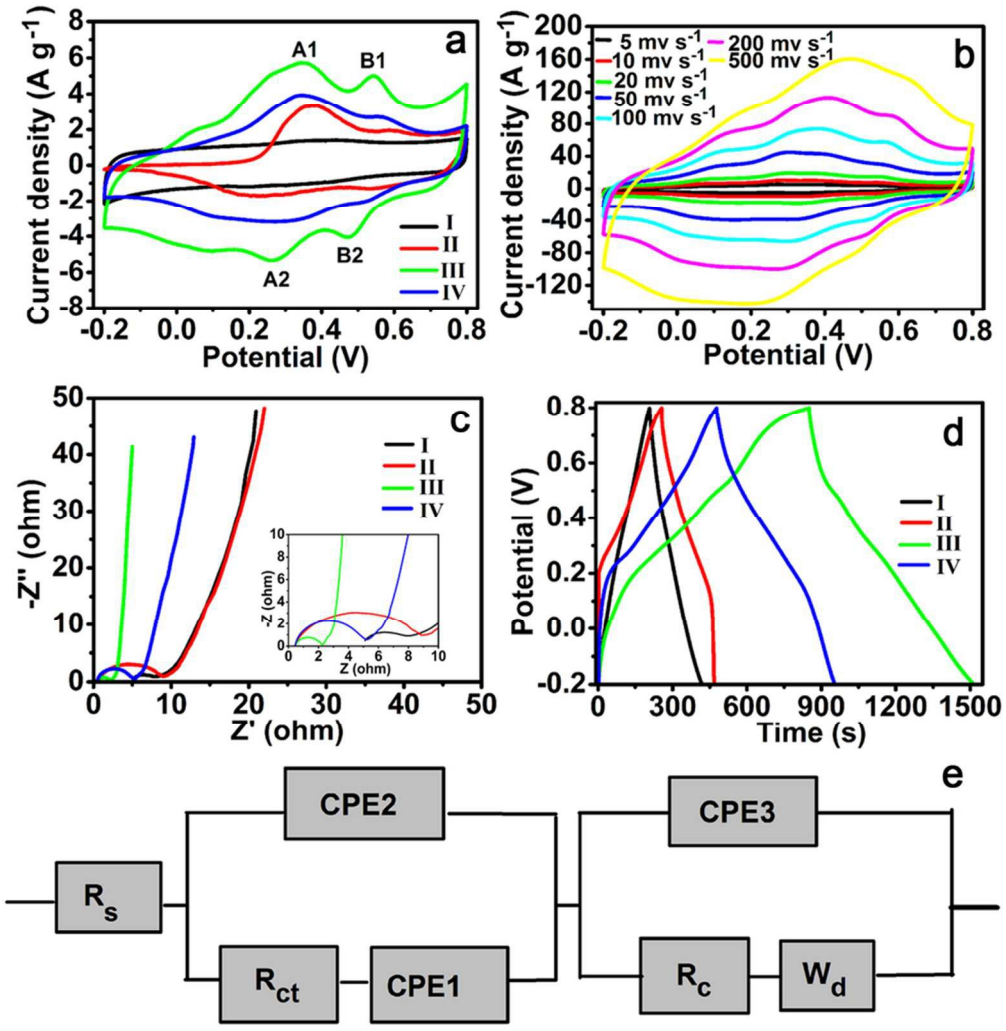

Fig. 4 Electrochemical charcterization of different samples: (a) CV curves of different samples at a scan rate of 5 mV s-1, (b) CV curves of MC/PANI15 at different scan rates, (c) EIS spectra of different samples (The inset shows the enlarged spectra in high frequency region), (d) Galvanostatic CD curves of different samples at a current density of 1 A g-1. (e) Equivalent circuit for simulating the EIS spectra of the MC/PANI sample. (I-MC, II-pure PANI, III-MC/PANI15, IV-MC/PANI20).
82x85mm (300 x 300 DPI)

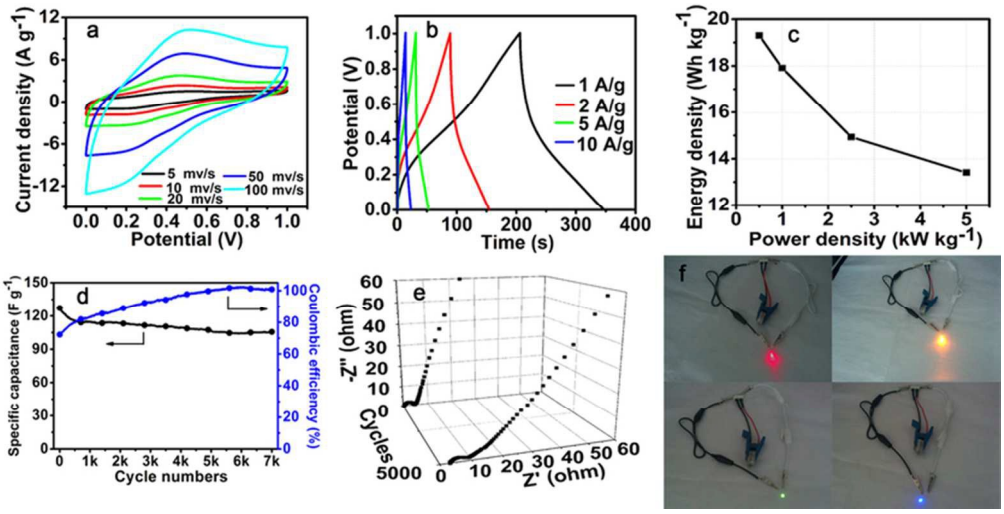

Fig. 5 (a) CV curves of the SC at different scan rates, (b) galvanostatic CD curves of the SC at different current densities, (c) Ragone plots of the symmetric SC device, (d) cycling performance and the corresponding Coulombic efficiency of the SC at a charge/discharge current density of 2 A g-1, (e) Nyquist plots of the SC before and after cycling test, (f) photographs of the LEDs driven by the SCs.
70x35mm (300 x 300 DPI)

Aligned polyaniline nanowires grown on internal surface of macroporous carbon for supercapacitors

Jianpeng Li, Yaqi Ren, Zhonghua Ren, Shuguang Wang, Yejun Qiu*, and Jie Yu*

Shenzhen Engineering Lab for Supercapacitor Materials, Shenzhen Key Laboratory for Advanced Materials, Department of Material Science and Engineering, Shenzhen Graduate School, Harbin Institute of Technology, University Town, Shenzhen 518055, China.

The table of contents entry:

Polyaniline nanowires grown on internal surface of macroporous carbon show high utilization efficiency for supercapacitors, leading high specific capacitance (1500 F g^{-1} at 1 A g^{-1})。